Detection of a gas flaring signature in the AERONET optical properties of aerosols at a tropical station in West Africa

Fawole, Olusegun G.; Cai, Xiaoming; Levine, James G.; Pinker, Rachel T.; Mackenzie, A. R.

DOI:
10.1002/2016JD025584

AGU PUBLICATIONS

JGR

Journal of Geophysical Research: Atmospheres

RESEARCH ARTICLE
10.1002/2016JD025584

Key Points:
- Classification of aerosol loadings into dominant source classes in the West African region
- Analysis of the optical and microphysical properties of major aerosol classes in the region
- First time identification/classification of gas flaring aerosol class signature in aerosol loading

Supporting Information:
- Supporting Information S1

Correspondence to:
A. R. MacKenzie,
a.r.mackenzie@bham.ac.uk

Citation:
Fawole, O. G., X. Cai, J. G. Levine, R. T. Pinker, and A. R. MacKenzie (2016), Detection of a gas flaring signature in the AERONET optical properties of aerosols at a tropical station in West Africa, *J. Geophys. Res. Atmos.*, *121*, doi:10.1002/2016JD025584.

Received 27 JUN 2016
Accepted 4 NOV 2016
Accepted article online 10 NOV 2016

The copyright line for this article was changed on 19 DEC 2016

Detection of a gas flaring signature in the AERONET optical properties of aerosols at a tropical station in West Africa

Olusegun G. Fawole[1,2], Xiaoming Cai[1], James G. Levine[1], Rachel T. Pinker[3], and A. R. MacKenzie[1,4]

[1]School of Geography, Earth and Environmental Sciences, University of Birmingham, Birmingham, UK, [2]Department of Physics and Engineering Physics, Obafemi Awolowo University, Ile-Ife, Nigeria, [3]Department of Atmospheric and Oceanic Science, University of Maryland, College Park, Maryland, USA, [4]Birmingham Institute of Forest Research, University of Birmingham, Birmingham, UK

Abstract The West African region, with its peculiar climate and atmospheric dynamics, is a prominent source of aerosols. Reliable and long-term in situ measurements of aerosol properties are not readily available across the region. In this study, Version 2 Level 1.5 Aerosol Robotic Network (AERONET) data were used to study the absorption and size distribution properties of aerosols from dominant sources identified by trajectory analysis. The trajectory analysis was used to define four sources of aerosols over a 10 year period. Sorting the AERONET aerosol retrievals by these putative sources, the hypothesis that there exists an optically distinct gas flaring signal was tested. Dominance of each source cluster varies with season: desert-dust (DD) and biomass burning (BB) aerosols are dominant in months prior to the West African Monsoon (WAM); urban (UB) and gas flaring (GF) aerosol are dominant during the WAM months. BB aerosol, with single scattering albedo (SSA) at 675 nm value of 0.86 ± 0.03 and GF aerosol with SSA (675 nm) value of 0.9 ± 0.07, is the most absorbing of the aerosol categories. The range of Absorption Angström Exponent (AAE) for DD, BB, UB and GF classes are 1.99 ± 0.35, 1.45 ± 0.26, 1.21 ± 0.38 and 0.98 ± 0.25, respectively, indicating different aerosol composition for each source. The AAE (440–870 nm) and Angström Exponent (AE) (440–870 nm) relationships further show the spread and overlap of the variation of these optical and microphysical properties, presumably due in part to similarity in the sources of aerosols and in part, due to mixing of air parcels from different sources en route to the measurement site.

1. Introduction

Some of the reservoirs from which crude oil is explored from the Earth's crust contains natural gas. This natural gas is separated at flow stations in the several oil and gas fields in every oil producing region of the world. This gas could be put to meaningful use (for example, power generation, domestic, and industrial uses). Where the infrastructure, technology, and/or market to put the gas to meaningful use are not available, the gas is either flared or vented into the atmosphere. Considering the climate forcing potential of methane, a major component of the gas, flaring is the better option. See *Fawole et al.* [2016] for a better understanding of the gas flaring process and its environmental impact. Gas flaring is the process of disposing of natural gas by combustion in an open flame in the open atmosphere, using a burner tip designed specifically for that purpose, in the course of routine oil and gas production operations. Flaring is most often associated with Nigeria and Russia, but it still takes place even in more developed economies, such as the case of the North Dakota Bakken shale region. The intensity of gas flaring and specifics of atmospheric transport can combine to enhance the role of gas flaring emissions over very large areas.

Gas flaring remains a significant source of air pollutants such as aerosol sulfate, black carbon (BC, colloquially "soot"), carbon monoxide (CO), polyaromatic hydrocarbon (PAH), and volatile organic compounds (VOCs), especially in those regions without the technical infrastructure needed to trap and process natural gas associated with oil reserves [*Fawole et al.*, 2016]. Tracking these aerosols from the source requires an understanding of the chemical character of the source and the prevailing meteorological conditions [*Eck et al.*, 2010; *Giles et al.*, 2012; *Rozwadowska et al.*, 2010]. With atmospheric residence times of 5–8 days, gas flaring associated aerosol, especially black carbon (BC), is a good tracer for gas flaring emissions [*Shindell et al.*, 2008]. This study aims to assess and quantify the contributions of intense gas flaring activities in the Nigeria oil field

to regional aerosol loadings. Gas flaring is a prominent contributor to atmospheric aerosol loading, on both local and regional scales, in leading oil producing nations of the world, including Russia, Nigeria, the USA, Iran, and Iraq [*Doherty et al*., 2014; *Fawole et al*., 2016].

Aerosol in the atmosphere can be classified in many different ways; here it is useful to consider fine- and coarse-absorbing classes, based on their radiation absorption potential and Mie-scattering particle-size equivalence [*Mielonen et al*., 2009]. The spectral dependence of aerosol optical and microphysical properties derived from remote sensing measurements of aerosol properties have been used to establish dominant aerosol signals [e.g., *Giles et al*., 2012; *Russell et al*., 2010]. Aerosol nature and properties vary with region; so adequate knowledge of major sources of aerosol in a region should enhance identification of dominant aerosol types at a measurement site in the region. Back trajectory analysis and adequate knowledge of the sources contributing to aerosol loadings in a region can, therefore, give a clearer understanding of the properties of the aerosol from the dominant sources [*Milinevsky et al*., 2014].

The Aerosol Robotic Network (AERONET) consists of more than 400 sites distributed around the globe. This network of automated Sun photometers has provided retrievals of aerosol properties for more than 20 years at some sites [*Holben et al*., 1998; *Holben et al*., 2001]. Many studies have utilized aerosol retrievals from the AERONET data set to analyze optical properties and size distribution and, hence, composition of aerosols in different regions of the world [e.g., *Giles et al*., 2012; *Kim et al*., 2011; *Milinevsky et al*., 2014; *Russell et al*., 2010; *Sato et al*., 2003].

Previous studies have classified the Ilorin AERONET site in West Africa, described in more detail below, as either a predominant dust [*Lee et al*., 2010; *Pandithurai et al*., 2001; *Pinker et al*., 2010; *Smirnov et al*., 2002] or mixed aerosol [*Eck et al*., 2010; *Giles et al*., 2012] site. The location of Ilorin (Figure 1) as the boundary city between the densely populated and industrialized Monsoonal forest region of the south and Savanah region of the north of Nigeria places it at a strategic location for aerosol-climate interactions. The prevailing winds are the dry northeasterly "Harmattan" (NEH) and moist southwesterly monsoon (SWM) winds. The SWM wind is the predominant wind during the WAM season. NEH brings dry Harmattan dust from the Sahara and Sahel region, usually between late November and early February, while the SWM brings in moist cool air that gives rain [*Sultan and Janicot*, 2003] but which may also carry urban and industrial aerosols from the south.

Gas flaring, the disposal of natural gas through stacks in an open-air flame, has been identified as a substantial, distinctive, and persistent source of atmospheric aerosol and pollutant trace gases [*Fawole et al*., 2016; *Huang et al*., 2015; *U.S. Environmental Protection Agency*, 2012]. Atmospheric pollutants emitted from gas flaring include CO, SO_2, PAH, VOCs, and black carbon (BC). To the south of the Ilorin AERONET site is the gas flaring region in Nigeria with over 300 active flare sites [*Anejionu et al*., 2015a; *Elvidge et al*., 2015] and an estimated annual average volume flared of 15 bcm (billion cubic meters). In the region, gas flaring is a daily routine at many of the sites, owing to the large amounts of natural gas produced, and inadequate piping to facilitate bringing the product to the market. Nigeria, presently ranked the second leading gas flaring nation of the world, is estimated to flare about 25% of its annual gas production [*Ite and Ibok*, 2013]. Figure 1 shows the spatial distribution of active flare sites in the Niger Delta, Nigeria, and location of the Ilorin AERONET site. In 2012, of the 325 active flare sites identified in the Nigeria oil field, 97 (~30%) ranked among the top 1000 largest flares identified globally. *Anejionu et al*. [2015b], in their analysis of the multiyear spatial dispersion of gas flaring gaseous emissions from the Niger Delta region, classified the airshed of more than 70% of the Niger Delta as moderate to high-pollution risk areas. *Giwa et al*. [2014], using emission factors from literature, estimated that gas flaring contributes about 10 Gg of black carbon (BC) to ambient BC concentration in the Niger Delta annually.

In the present study, using a combination of trajectory analysis and knowledge of dominant aerosol sources in the region, we created clusters of dominant aerosol types at the site for 2005–2009 and 2011–2015. The statistics of the optical properties of these measurement clusters were then analyzed for aerosol optical depth (AOD), Absorption Angström Exponent (AAE), Angström Exponent (AE), single scattering albedo (SSA) and fine mode fraction (FMF). See *Dubovik and King* [2000], *Dubovik et al*. [2000], and *Holben et al*. [2006] for a full description of the derivation of these metrics from both direct Sun radiance and sky radiances measured by ground-based Sun-sky scanning radiometers at AERONET sites globally.

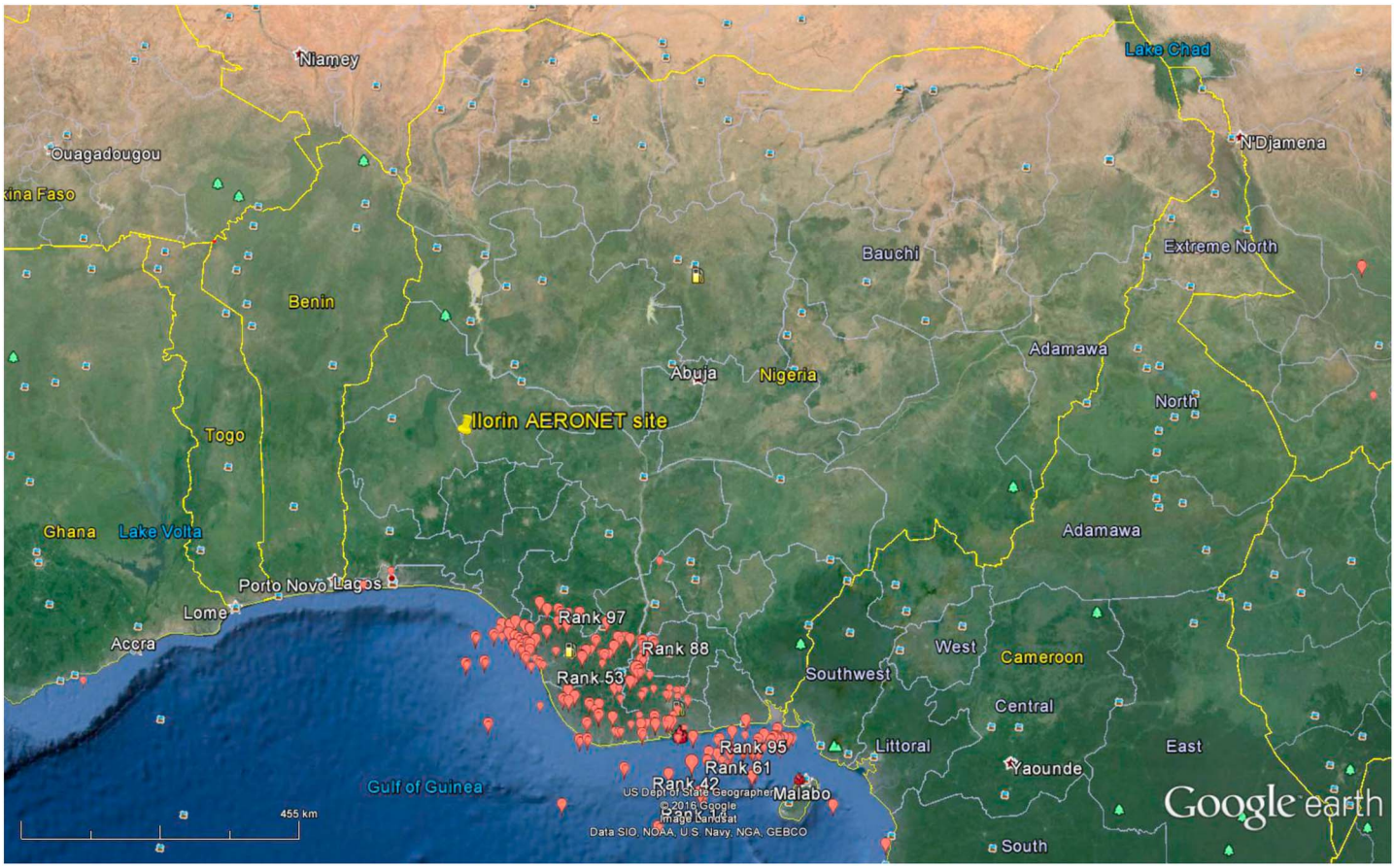

Figure 1. Google Earth image showing location of Ilorin AERONET site and the cluster of gas flaring sites in the Niger Delta, Nigeria.

2. Methodology

2.1. Description of the AERONET Site and Major Sources of Aerosol

The AERONET site is located in Ilorin, Nigeria (8.32°N, 4.34°E) (Figure 1). Ilorin has a tropical wet and dry/savannah climate. Based on the Köppen-Geiger climatic classification, Ilorin can be classified as equatorial savannah with dry winter (Aw). In Ilorin, the annual mean rainfall and temperature are about 1220 mm and 26.5°C, respectively [*Olaniran*, 1982; *Tunde et al*., 2013]. The region has two big cities—Lagos and Oyo, city regions with populations of 17 and 5 million, respectively—and the gas flaring region (Niger Delta) to the south, the Sahel and Sahara region to the north and major sources of biomass burning emissions in West Africa to the east and west. The movement of the Intertropical Convergence Zone (ITCZ) and Intertropical Front (ITF) determines the preonset and onset of the West African Monsoon (WAM) in the region. Biomass burning emissions are intense in the region between November and March [*Roberts et al*., 2009], a period during which there is also significant dust transport from the Sahel and Sudan region. Saharan dust is predominant between late November and January, a period of intense Harmattan conditions. Depending on the season and prevailing meteorological conditions, there is an influx of urban and industrial aerosols from the south. We expect this influx of urban-industrial air to predominate during the WAM months, between April and October. We hypothesize that aerosols from each of these sources exhibit statistically significant differences in their optical—and, hence, microphysical—properties.

Figure 1 shows the locations of the Ilorin AERONET site and dense concentration of gas flaring sites in the Niger Delta area, Nigeria. The brown area shown in Figure 1 is the Sahara and Sahel regions, which is the major sources of dust in the region. Data for the locations of the gas flaring sites were obtained from the supporting information in *Elvidge et al*. [2015].

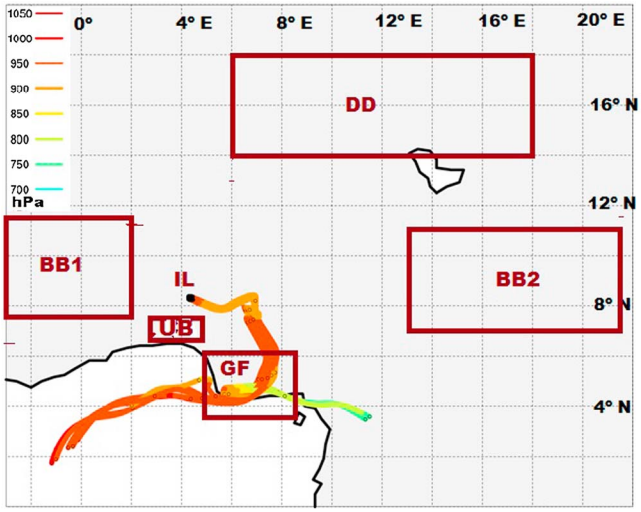

Figure 2. An example of trajectory plot together with the areas of major aerosol sources and the AERONET site (BB, DD, UB and, GF represent biomass emissions, desert dust, urban, and gas flaring sources, while IL indicates the AERONET site at Ilorin, Nigeria).

2.2. Trajectory Calculation and Classification

For the months when AERONET data were available for the site over the period considered, 2005–2015 (excluding 2010), 7 day back trajectories were calculated using the UK Universities Global Atmosphere Modelling Programme (UGAMP) offline trajectory model. This model is driven by 6-hourly ERA-Interim (European Centre for Medium-Range Weather Forecasts Interim Reanalysis) wind analyses data. Three-dimensional meteorological data are interpolated to the trajectory locations. For each integration time, values of meteorological fields (temperature, potential temperature, and pressure) are assigned as attributes to the particle in the trajectory. Detailed technical descriptions of the UGAMP trajectory model can be found in *Methven* [1997] and *Methven et al.* [2001].

Nine (9) backward trajectories spaced 0.05° × 0.05° (i.e., 5 × 5 km) apart on a 0.1° × 0.1° grid were released 6 hourly, that is, at 0000, 0600, 1200, and 1800, at 900 hPa (i.e., approximately 1.5 km altitude) on each of the days for which the calculations were done. It must be noted that these trajectories, in general, change altitude as a function of transit time: 900 hPa is the arrival pressure at the AERONET site. The choice of 7 day back trajectory length is due to the atmospheric lifetime of between 5 and 9 days estimated for black carbon (BC) and particulate organic matter [*Cooke et al.*, 1997; *Cooke and Wilson*, 1996; *Koch et al.*, 2009; *Stier et al.*, 2006], both of which are major constituent of aerosol in the study area. Desert dust is also a prominent aerosol constituent, especially during the non-WAM months.

The clustering of the aerosol signals by their trajectory paths enables a consideration of the major sources of aerosol in the region as shown in Figure 2. See earlier studies [e.g., *Omar et al.*, 2005; *Russell et al.*, 2014] for more on the clustering of aerosol parameter using AERONET data. In this study, the classification was based solely on the trajectory coordinates, considering whether the trajectory had passed through the gridded regions of one or more of the major aerosol sources where they are suggested to have picked up aerosol signatures peculiar to such sources. The classification algorithm developed and used in this study allows the large data set (10 years of trajectories) to be processed automatically avoiding manual inspection of trajectory maps.

When at least six of the nine trajectories released at a point in time pass through one of the source region, that region is considered to be the dominant source of the aerosol signal measured. When there are an almost equal number of trajectories from two sources in the four sets of 6-hourly trajectories released on a day, the aerosol signal recorded on that day is regarded as a mixture of the two most dominating sources. In this way, eight clusters were created: BB, DD, UB, GF, DD-BB, DD-UB, GF-UB, and GF-DD. BB-UB and BB-GF clusters occurred less than 1% of the time and are therefore not investigated further. In this study, we analyze the optical properties of BB-, UB-, GF-dominant and "pure" DD clusters as well as their climatologies. Box plots presenting variation of optical and microphysical properties of the "mixed-source clusters" are available in the supporting information (see Figure S1). Because AERONET measurements observe the aerosol through the depth of the atmosphere, differential advection with height can bring air of different origins above the site simultaneously. We do not attempt to quantify this and limit our study to finding dominant sources in air arriving close to the surface (900 hPa).

2.3. AERONET Data

AERONET network provides Sun photometer measurements of AOD at up to eight wavelengths between 340 and 1020 nm. The network has been in operation since mid-1990s [*Holben et al.*, 1998] and currently with over

400 sites globally [*Chubarova et al*., 2016]. It also measures the angular distribution of sky radiance at four wavelengths (0.44, 0.67, 0.87, and 1.02 μm). An inversion algorithm is used for the retrieval of optical and microphysical properties of atmospheric aerosols, such as volume size distribution, asymmetric parameter (g), complex refractive index (m), and single scattering albedo (SSA) at 0.44, 0.67, 0.87, and 1.02 μm [*Dubovik et al*., 2002; *Dubovik and King*, 2000; *Eck et al*., 2010]. For sites like Ilorin where differences in the diurnal variation of aerosol are very pronounced, the use of monthly averages of aerosol parameters will provide only highly generalized estimates of the optical and microphysical properties of aerosol at such a site.

The Angström Exponent (AE), a measure of the wavelength (λ) dependence of aerosol optical depth (τ), indicates the dominant aerosol size because the spectral shape of the extinction is inversely related to the particle size [*Eck et al*., 1999; *Schuster et al*., 2006]. The wavelength dependence of scattering as quantified by AE (α) is given by equation (1):

$$\propto = -\frac{\ln\left(\tau_{\lambda 1}/\tau_{\lambda 2}\right)}{\ln\left(\lambda_1/\lambda_2\right)}. \tag{1}$$

Level 1.5 of Version 2 AERONET retrievals were used in the analyses of the optical and microphysical properties of the clusters because Level 2 data, especially inversion products, were not sufficiently available. Level 2 data of aerosol parameters from the Ilorin AERONET site were used to analyze the dynamics of the seasonal variation of fine-mode fraction (FMF), AOD, and AE (470–870 nm) [*O'Neill et al*., 2003]. Although, Level 1.5 data are cloud screened, to further enhance the quality of the Level 1.5 data used in this analysis, we have included only Level 1.5 data for which Level 2 size distribution data are available. This restriction ensures that only Level 1.5 data for which solar zenith angle $> 50°$ are used in the analysis [see *Bond et al*., 2013; *Dubovik et al*., 2002]. According to *Dubovik et al*. [2000], SSA values get worse when AOD (440 nm) ≤ 0.2. Hence, we have used a threshold value of AOD (440 nm) > 0.2 in this analysis. The quality control approach adopted, as stated above, implies that we have applied the same quality control check for Level 2 retrievals except that we have relaxed the AOD (440 nm) requirement from 0.4 to 0.2.

The variation of absorption aerosol optical thickness (τ_{abs}) with wavelength (λ) can be approximated with a logarithmic wavelength dependence to infer the Absorption Angström Exponent, AAE, (α_{abs}), as given in equation (2). Similarly, as given in equation (3), the Extinction Angström Exponent, EAE, (α_{ext}) is obtained from the spectral dependence of extinction aerosol optical thickness (τ_{ext}) with wavelength (λ) on a logarithmic scale.

$$\alpha_{abs} = -\frac{d\ln[\tau_{abs}(\lambda)]}{d\ln(\lambda)} \tag{2}$$

$$\alpha_{ext} = -\frac{d\ln[\tau_{ext}(\lambda)]}{d\ln(\lambda)}. \tag{3}$$

The spectral single scattering albedo (SSA) of an aerosol, as given in equation (4), is the ratio of scattering to extinction (the sum of absorption and scattering). SSA depends on the strength of the absorption of the aerosol sources and the aging of the aerosol during atmospheric transport. For atmospheric aerosols, the value of SSA and AOD primarily determines the sign and magnitude of its radiative forcing, respectively.

$$\omega = \frac{\sigma_{sca}}{\sigma_{ext}} = \frac{\sigma_{sca}}{\sigma_{sca} + \sigma_{abs}} \tag{4}$$

2.4. Climatic Condition at the Study Site

The predominant seasons at the site are governed by the movement of the Intertropical Convergence Zone (ITCZ) and Intertropical Front (ITF). The ITF is the northern limit of the southwesterly winds of the monsoon. The preonset stage of the West African Monsoon (WAM), usually between May and June, is characterized by the movement of the ITF further north to 15°N which brings in the first period of rain. A further shift of the ITF to its northernmost position around 20°N takes place between July and August, a period which signifies the onset of WAM [*Sultan and Janicot*, 2000; *Sultan and Janicot*, 2003]. At the onset of the WAM, there is an abrupt shift in the latitudinal position of the ITCZ from a location of 5°N in May–June to a location at 10°N in July–August.

2.5. Statistical Analysis

For statistical analysis of aerosol optical and microphysical properties, the SPSS statistics package 22 (SPSS Inc., Chicago, IL, USA) was used. The mean values and variability of AAE and AE for all four clusters—DD,

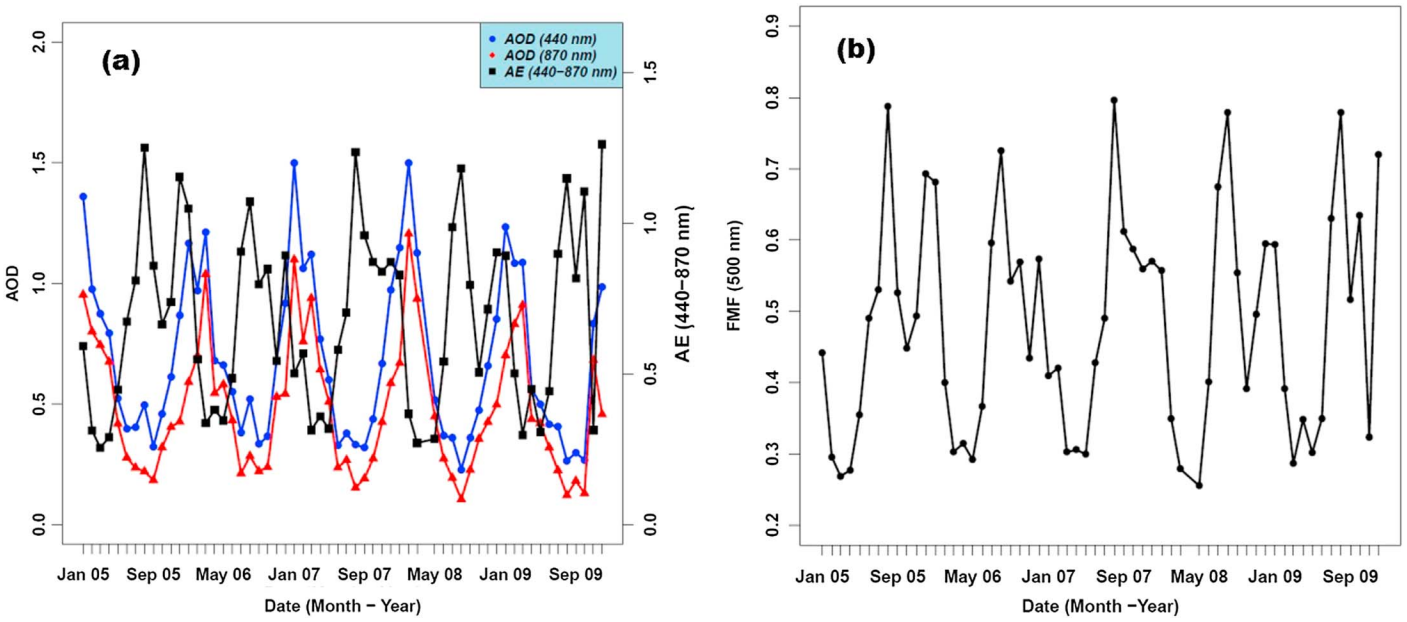

Figure 3. Temporal variation of monthly averages of (a) AOD at 440 nm and 870 nm and (b) AE (440–870 nm) FMF (500 nm).

BB, UB, and GF—were compared pairwise to establish the statistical significance of the differences between these mean values. For statistical analysis, the clusters were paired as follows for comparison: (a) UB-GF, (b) GF-BB, (c) UB-BB, (d) BB-DD, (e) UB-DD, and (f) GF-DD. The results and discussion of the statistical analysis are presented in the supporting information.

3. Results and Discussions

3.1. Dynamics of Seasonal Variation of AOD and AE

During the preonset and onset of the WAM (May–September), there is a sharp decrease in the average monthly AOD (440 nm) by a factor of about 4 from 1.22 ± 0.17 in DJF (December–February) to 0.35 ± 0.06 in JJA (June–August) over the 5 year period (2005–2009) considered in Figure 3a. This is arguably due to the northward shift of the ITCZ and ITF (as discussed in section 2.4) which cuts off the intense intrusion of Saharan dust but increases the inland flow of SWM wind. The end of the biomass burning season could be a contributor to the decrease in AOD. The SWM wind brings aerosol from the large cities (urban, UB) and industries (including gas flaring, GF) upwind of the AERONET site. As shown in Figure 3b, fine-mode aerosol fraction dominates (FMF > 0.7) the period of low AOD (June–September, JJAS): combustion—biomass burning, biofuel, vehicular, and fossil—emissions are major sources of fine-mode aerosol fraction.

Figure 3a presents the temporal variation of the average monthly AE for the period 2005–2009. Low AOD periods are associated with high AE values (>0.7) which is typical of combustion aerosols like fossil fuel and biomass burning. In the region, biomass burning is predominantly between November and March which does not overlap with the low AOD period.

The monthly average AOD pattern is shown in Figure 3a for 440, 675, and 870 nm. For the analysis of the daily variation of AOD and AE, this 5 year period (2005–2009) was chosen because there were very few missing data during these years. At the Ilorin AERONET site, there are frequent breaks in data availability probably due to adverse meteorological conditions, for example, persistent cloud cover or instrument breakdown.

Figure 4 presents the distribution of the daily AOD (440 nm) and AE (440–870 nm) between 2005 and 2009 for both the WAM and non-WAM months. In these classifications, the WAM months are April–October, while the non-WAM months are November–March. All four histograms are positively skewed. For the WAM months, the AOD distribution is less skewed. The median values of AOD (440 nm) is 0.48 and 0.95 for the WAM and non-WAM months, respectively.

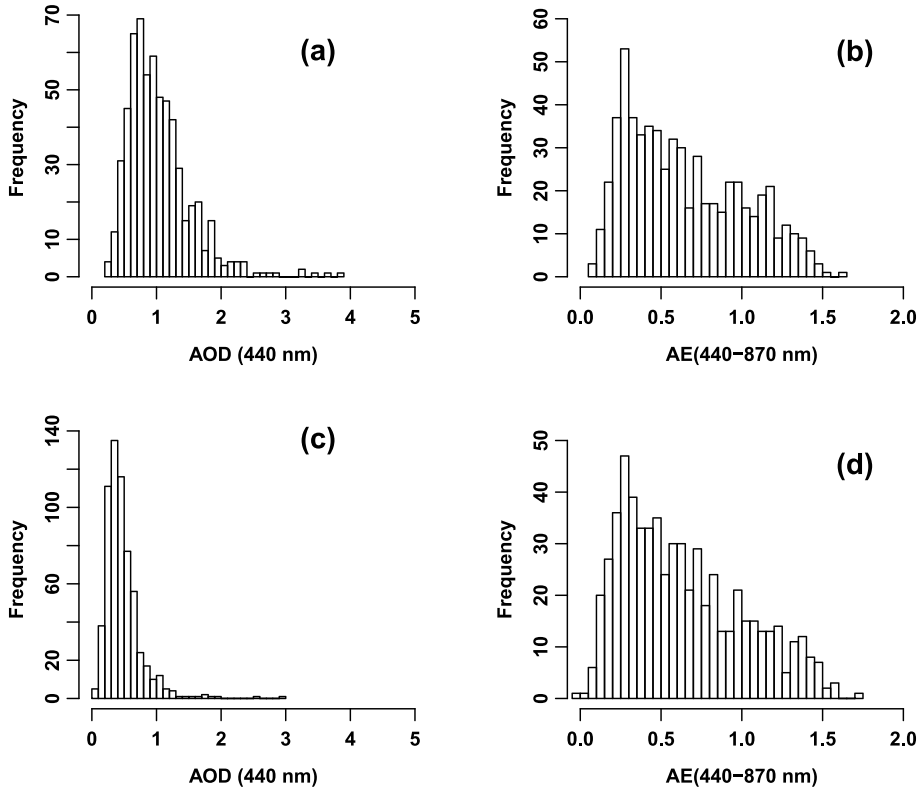

Figure 4. Distribution of daily variation of (a) AOD (440 nm) and (b) AE (440–870 nm) for non-WAM months; (c) AOD (440 nm) and (d) AE (440–870 nm) for WAM months over a 5 year period (2005–2009). For AOD plots, bin widths are ~0.1 units of AOD.

During the WAM months, the several spikes observed in the daily AOD data are most likely due to local dust rather than dust transport from the Sahara. In contrast to cities in the developed economies, there is a dominance of the coarse-mode fraction in the atmospheric aerosol loading in major Nigerian cities. This has been attributed to frequent and persistent resuspension of dust from the large expanse of unpaved roads [*Akinlade et al*., 2015; *Obioh et al*., 2013; *Owoade et al*., 2013].

3.2. Seasonal Dynamics of Aerosol Absorption: Single Scattering Albedo (SSA)

Single scattering albedo (SSA) of atmospheric aerosols is an important parameter in estimating the radiative effect of the aerosol. Depending on the surface reflectance (albedo), SSA determines the sign of the radiative effect, hence its cooling/warming potential; it ranges from 0 (zero) for a purely absorbing aerosol to 1 for a purely scattering aerosol.

During the WAM months, the average monthly SSA decreases with wavelength (see the green ellipses in Figure 5), and slightly increases with wavelength during the non-WAM months (DJF). This decrease, between 5.2 and 5.7%, is attributable to the fact that scattering often decreases faster than absorption with wavelength for carbonaceous particles [*Bergstrom et al*., 2007]. SSA is also highest during these months for the 5 year period shown in Figure 5, due presumably to increased concentrations of less absorbing particles in the aerosol influx from the urban and gas flaring (industrial) regions downwind of Ilorin. SO_2, a precursor gas for atmospheric sulfate, is a major pollutant from gas flaring of "sour" natural gas sources [*Fawole et al*., 2016]. Mixtures of sulfate and BC (carbonaceous particles) have been associated with high SSA values [*Lim et al*., 2014].

3.3. Optical and Microphysical Properties of Aerosol Clusters

Figure 6 presents scatterplots of AAE (440–870 nm) versus AE (440–870 nm), and AAE (440–870 nm) versus FMF (500 nm), to show the range of unique optical and microphysical properties exhibited by the different clusters created from the trajectory and source analysis. Scatterplots such as these have been used to classify

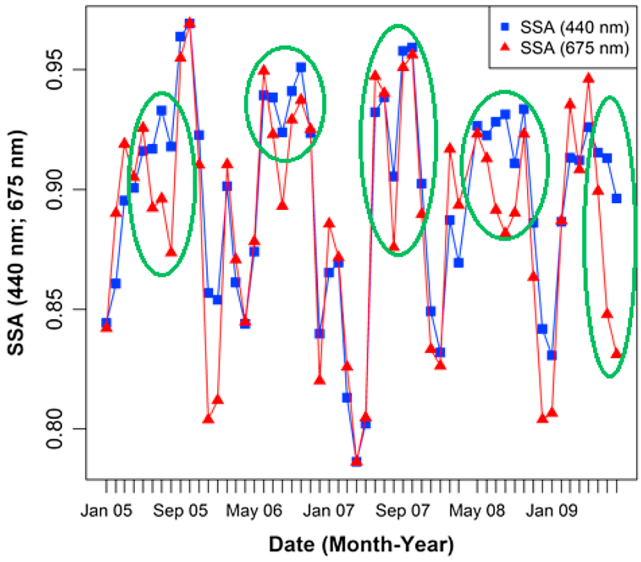

Figure 5. Multiyear (2005–2009) seasonal variation of SSA at 440 and 675 nm. Green ellipses denote times, during the WAM months, when SSA decreases with wavelength.

aerosol loadings, measured remotely by Sun photometers, in terms of their dominant compositions, nature, and potential origin [*Dubovik et al.*, 2002; *Milinevsky et al.*, 2014; *Russell et al.*, 2010].

Of the total number ($N = 801$) of aerosol signatures assigned to the various clusters, BB-, UB-, GF-dominant and pure DD account for 184 (23%), 212 (26.5%), 167 (20.8%), and 238 (29.7%), respectively. This suggests that gas flaring (GF) is a major contributor to the aerosol signature in the region, especially during the WAM months. The number of trajectories classified into each of the "mixed clusters" is as follows: UB-GF ($N = 145$), GF-DD ($N = 55$), DD-UB ($N = 63$), and BB-DD ($N = 119$). The mixed clusters are not discussed further in this study.

3.3.1. Desert Dust (DD) Aerosol Cluster

Desert dusts are predominant in the region with the coming of the NEH wind usually between late November and February when both the ITCZ and ITF are nearer the equator. The DD cluster is associated with high AOD (median = 1.02; Q1 and Q3 are 0.72 and 1.32, respectively): the association of high AOD and low AE is typical of desert dust [*Toledano et al.*, 2007].

As presented in Table 1a, for the DD cluster, the range of values for the AAE, and AE are $1.64 \leq \alpha_{abs} \leq 2.34$ and $0.19 \leq \alpha_{ext} \leq 0.49$, respectively. These values corroborate findings from similar sites [*Giles et al.*, 2012; *Russell et al.*, 2010]. The absorption potential of desert dust as shown in the SSA_{440} values $\omega = 0.90 \pm 0.03$ is determined by the hematite (iron oxides) content of desert dust, which is a strong determinant of the radiative

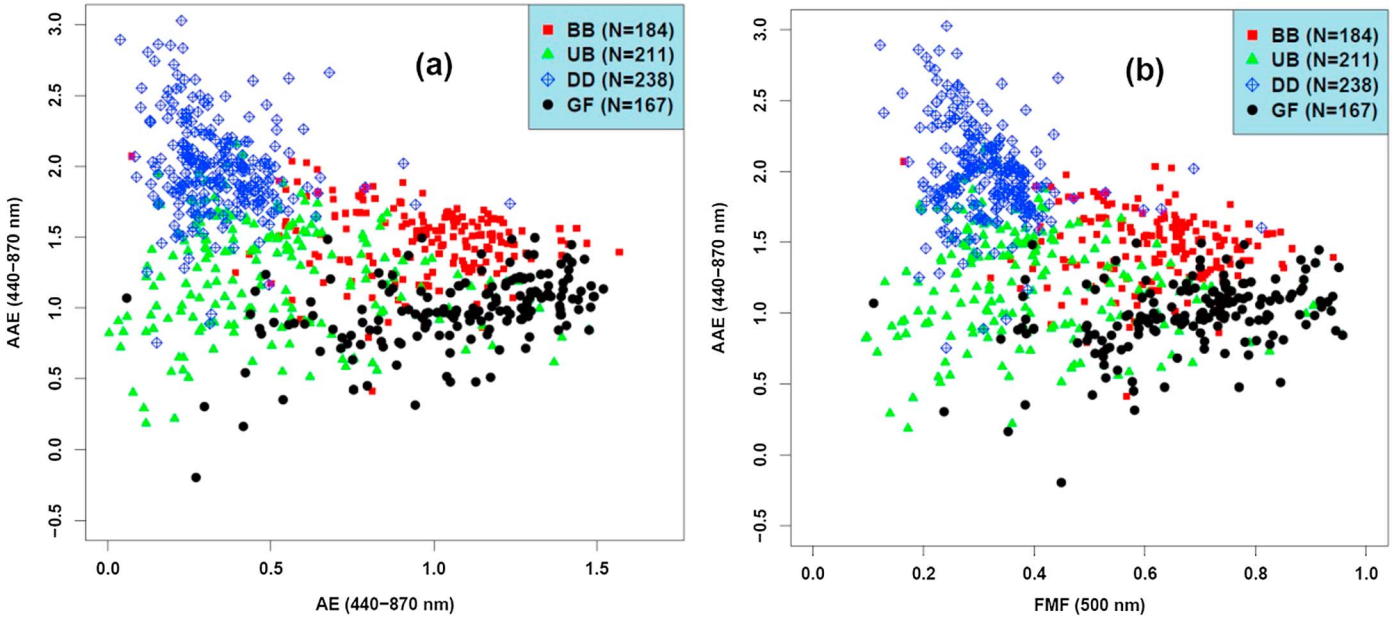

Figure 6. Scatterplot of (a) AAE (440–870 nm) versus AE (440–870 nm). (b) AAE (440–870 nm) versus FMF (500 nm) for the four identified aerosol clusters.

Table 1a. Mean Optical and Microphysical Properties of the Aerosol Clusters[a]

Aerosol Properties	BB	UB	GF	DD
AAE (440–870)	1.45 (0.26)	1.21 (0.38)	0.98 (0.26)	1.99 (0.35)
AE (440–870)	0.98 (0.25)	0.57 (0.35)	1.07 (0.30)	0.34 (0.15)
FMF (500 nm)	0.63 (0.12)	0.41 (0.18)	0.68 (0.16)	0.31 (0.08)
SSA (675 nm)	0.86 (0.04)	0.92 (0.04)	0.90 (0.06)	0.95 (0.02)

[a]The values in parentheses are standard deviations showing the spread of the values.

effect of the aerosol. SSA_{440} is given here because iron oxide absorbs much more in the shorted wavelength. As expected for aerosol in this cluster, the AE values show a dominance of the coarse-mode fraction. Hence, this cluster can be referred to as coarse absorbing.

3.3.2. Biomass Burning (BB) Aerosol Cluster

Aerosol in this cluster is predominant in the months before the preonset of the WAM, i.e., between November and March. In West Africa, March is usually the peak of the dry season and, as such, intense agricultural burning takes place between November and March to prepare the land for planting during the forthcoming rainy season. Intrusion of desert dust is also a regular occurrence within this period. The trajectory clustering enabled us to identify days of dominance of both aerosol signatures with these months (November–March). There are days of an almost equal contribution of trajectories from these sources (DD and BB) to the back trajectory analysis. Such days are categorized as a mixture from both sources, that is, DD-BB.

The BB cluster is characterized by high AOD and high AE values; the high AE value is evident in the EAE values shown in Table 1a. The high carbon content of biomass burning aerosols is responsible for its high absorbing nature as expressed by its SSA_{675} values ($\omega = 0.86 \pm 0.04$), the lowest of the four clusters. The ranges of the AAE and AE values are $1.19 \leq \alpha_{abs} \leq 1.71$ and $0.73 \leq \alpha_{ext} \leq 1.23$, respectively. This cluster, similar in value to other biomass burning sites in the literature, has a relatively high FMF value, while the AE value for this cluster is slightly lower than expected. This probably relates to the nature of vegetation burned, the aging of aerosol during transport to the measurement site, or a slight contribution from dust, mixed-in or aloft.

3.3.3. Urban Aerosol (UB) Aerosol Cluster

Urban (UB) aerosol signatures are predominant in the trajectory classification between May and October; it is often intense between June and September (JJAS). This is due to northward shift of the ITCZ and ITF (as discussed in section 2.4) which allows inland influx of moist SWM wind that brings rain. This wind brings pollution laden aerosol from the large cities, Lagos and Oyo, with high human population densities.

The UB cluster has an average SSA_{675} value of 0.92 ($\pm$0.04), that is, it is relatively more absorbing than the DD cluster due to the presence of carbonaceous particles from combustion processes and vehicular emissions. The range of AAE values, $0.83 \leq \alpha_{abs} \leq 1.59$, is very similar to observations from similar urban sites [*Giles et al*., 2012]. The average AE value, compared to similar sites in literature, is lower by a factor of 2.5 which suggests the dominance of coarse-mode particles. This lower AE values are attributable to dust resuspension from the predominantly unpaved and damaged paved road networks that lie across major cities in Nigeria. Several in situ PM measurements across various site classifications (residential, marine, heavy traffic, and industrial) in major Nigeria cities have reported the dominance of the coarse-mode ($PM_{2.5\text{-}10}$) PM fraction [*Akinlade et al*., 2015; *Ezeh et al*., 2012; *Obioh et al*., 2013; *Owoade et al*., 2013].

3.3.4. Gas Flaring (GF) Aerosol Cluster

The gas flaring region, about 500 km south of the AERONET site, contains no fewer than 300 flaring sites scattered around the Niger Delta, a land mass of about 70, 000 km^2 [*Anejionu et al*., 2014; *Elvidge et al*., 2015]. *Onyeuwaoma et al*. [2015], studying aerosol loading patterns in major Nigerian cities from Moderate Resolution Imaging Spectroradiometer and OMI data, identified gas flaring from the oil and gas fields in the Niger Delta area as a contributor to elevated concentrations of carbon monoxide (CO) observed in cities near the flaring region. Wind trajectories from the gas flaring region are captured in the trajectory analysis predominantly during the WAM months.

Of the four dominant clusters identified, aerosols in the GF cluster have the lowest average AAE value of 0.98. This value, which is very close to the theoretical AAE value of 1 associated with BC [*Bergstrom*, 1973; *Bohren and Huffman*, 1983], is attributed to the BC component of gas flaring aerosols. There is some overlap in the

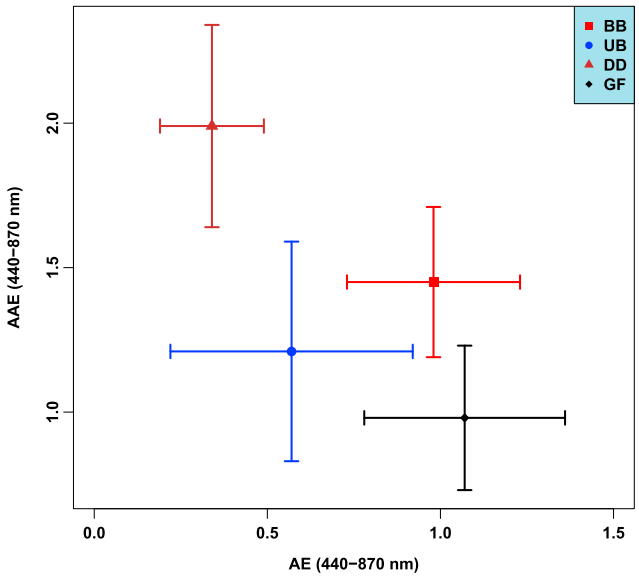

Figure 7. Scatterplot with *X* and *Y* error bars for the AAE versus AE mean values for the four aerosol classes. The error bars represents the standard deviations.

AAE values of the BB and GF clusters, probably due to both having substantial carbonaceous particle content. Although, as shown in Figure 7, the AE values for the BB and GF clusters overlap; the statistical comparison of the sample distributions shows that the means are significantly different (see supporting information). For the GF cluster, the ranges of the AAE and AE values are $0.72 \leq \alpha_{abs} \leq 1.24$ and $0.77 \leq \alpha_{ext} \leq 1.37$, respectively. See the supporting information (Figure S2) for box plots showing the spread and overlap of the different properties for the four clusters. The average SSA_{675} ($\omega = 0.9 \pm 0.06$) value for the GF cluster shows that it is more absorbing than the UB-dominant aerosol cluster. Like BB-dominated aerosol cluster, aerosols in this cluster can be referred to as fine absorbing.

Figure 7 shows the spread of the AAE and AE of the four aerosol clusters identified. DD-dominated aerosols are unique in terms of AAE and AE, while there are varying degrees of overlaps in those of UB, BB, and GF dominated aerosols. The statistical comparison of the mean values of AAE and AE for the four aerosol clusters is presented in the supporting information.

To examine the distribution of the aerosol parameters, Table 1b presents the median values of the optical and microphysical properties of the four aerosol clusters identified. The skewness of the distribution of these properties in all the clusters is very mild as shown by the closeness of the mean and median values of the aerosol parameters as shown in Tables 1a and 1b.

4. Conclusions

Earlier studies have classified the Ilorin AERONET site as dominated by dust or a mixture of dust and biomass burning aerosols. Analysis presented here for 10 years of aerosol data from this site allows, for the first time, the identification and analysis of contribution of dominant sources to the mixed aerosol loading at the site. The aerosol optical depth (AOD) and Angström Exponent (AE) vary significantly during the year due to a significant change in the nature and composition of dominant aerosols at the site. The months before the West African Monsoon (WAM) are characterized by aerosol with high AOD and low AE, while the WAM months witness aerosols with low AOD and high AE.

Back trajectories classification for the study period (2005–2009 and 2011–2015) and known major source contributors to aerosol loading in the region were used to create three aerosol-dominant (BB, UB, and GF) and one pure DD source-related clusters from AERONET retrievals, which vary significantly in optical and microphysical properties. Biomass burning and desert dust-dominant aerosols are prominent in the pre-WAM months, while gas flaring and urban aerosols dominate the WAM months.

Table 1b. Median Values of Optical and Microphysical Properties of the Clusters[a]

Aerosol Properties	BB	UB	GF	DD
AAE (440–870)	1.47 (1.27, 1.64)	1.21 (0.93, 1.5)	0.99 (0.87, 1.14)	1.98 (1.79, 2.18)
AE (440–870)	0.98 (0.78, 1.15)	0.51 (0.3, 0.79)	1.14 (0.95, 1.3)	0.3 (0.23, 0.41)
FMF (500 nm)	0.63 (0.53, 0.7)	0.38 (0.29, 0.53)	0.7 (0.59, 0.79)	0.3 (0.25, 0.35)
SSA (675 nm)	0.85 (0.83, 0.88)	0.93 (0.9, 0.96)	0.9 (0.84, 0.95)	0.95 (0.94, 0.97)

[a]Values in parentheses are the 25% and 75% percentiles.

The unique properties and contribution of gas flaring aerosol to the overall aerosol loading underpins the need for further studies on this "overlooked" source of aerosol. The optical and size properties identified for these clusters can be used to identify similar aerosol signatures for similar sites.

Acknowledgments
We appreciate the efforts of the PI for the Ilorin AERONET site for obtaining, processing, and making the data used in this study available. We also appreciate the anonymous reviewers for their comments and corrections that have helped to improve the quality of this paper. Olusegun G. Fawole is highly grateful to the UK government for funding his PhD studies through the UK Commonwealth Scholarship Commission (CSCUK). The data used in this analysis are available at http://aeronet.gsfc.nasa.gov/.

References

Akinlade, G. O., H. B. Olaniyi, F. S. Olise, O. K. Owoade, S. M. Almeida, M. Almeida-Silva, and P. K. Hopke (2015), Spatial and temporal variations of the particulate size distribution and chemical composition over Ibadan, Nigeria, *Environ. Monit. Assess.*, *187*(8), 1–14.

Anejionu, O. C. D., G. A. Blackburn, and J. D. Whyatt (2014), Satellite survey of gas flares: Development and application of a Landsat-based technique in the Niger Delta, *Int. J. Remote Sens.*, *35*(5), 1900–1925.

Anejionu, O. C., G. A. Blackburn, and J. D. Whyatt (2015a), Detecting gas flares and estimating flaring volumes at individual flow stations using MODIS data, *Remote Sens. Environ.*, *158*, 81–94.

Anejionu, O. C., J. D. Whyatt, G. A. Blackburn, and C. S. Price (2015b), Contributions of gas flaring to a global air pollution hotspot: Spatial and temporal variations, impacts and alleviation, *Atmos. Environ.*, *118*, 184–193.

Bergstrom, R. (1973), Extinction and absorption coefficients of the atmospheric aerosol as a function of particle size, *Contr. Atmos. Phys.*, *46*, 223–234.

Bergstrom, R. W., P. Pilewskie, P. Russell, J. Redemann, T. Bond, P. Quinn, and B. Sierau (2007), Spectral absorption properties of atmospheric aerosols, *Atmos. Chem. Phys.*, *7*(23), 5937–5943.

Bohren, C., and D. Huffman (1983), *Light Scattering and Absorption by Small Particles*, Wiley, New York.

Bond, T. C., S. J. Doherty, D. Fahey, P. Forster, T. Berntsen, B. DeAngelo, M. Flanner, S. Ghan, B. Kärcher, and D. Koch (2013), Bounding the role of black carbon in the climate system: A scientific assessment, *J. Geophys. Res. Atmos.*, *118*, 5380–5552, doi:10.1002/jgrd.50171.

Chubarova, N., A. Poliukhov, and I. Gorlova (2016), Long-term variability of aerosol optical thickness in Eastern Europe over 2001–2014 according to the measurements at the Moscow MSU MO AERONET site with additional cloud and NO_2 correction, *Atmos. Meas. Tech.*, *9*(2), 313–334.

Cooke, W. F., and J. J. Wilson (1996), A global black carbon aerosol model, *J. Geophys. Res.*, *101*(D14), 19,395–19,409, doi:10.1029/96JD00671.

Cooke, W. F., S. Jennings, and T. Spain (1997), Black carbon measurements at Mace Head, 1989–1996, *J. Geophys. Res.*, *102*(D21), 25,339–25,346, doi:10.1029/97JD01430.

Doherty, S. J., C. Dang, D. A. Hegg, R. Zhang, and S. G. Warren (2014), Black carbon and other light-absorbing particles in snow of central North America, *J. Geophys. Res. Atmos.*, *119*, 12,807–12,831, doi:10.1002/2014JD022350.

Dubovik, O., and M. D. King (2000), A flexible inversion algorithm for retrieval of aerosol optical properties from Sun and sky radiance measurements, *J. Geophys. Res.*, *105*(D16), 20,673–20,696, doi:10.1029/2000JD900282.

Dubovik, O., A. Smirnov, B. Holben, M. King, Y. Kaufman, T. Eck, and I. Slutsker (2000), Accuracy assessments of aerosol optical properties retrieved from Aerosol Robotic Network (AERONET) Sun and sky radiance measurements, *J. Geophys. Res.*, *105*(D8), 9791–9806, doi:10.1029/2000JD900040.

Dubovik, O., B. Holben, T. F. Eck, A. Smirnov, Y. J. Kaufman, M. D. King, D. Tanré, and I. Slutsker (2002), Variability of absorption and optical properties of key aerosol types observed in worldwide locations, *J. Atmos. Sci.*, *59*(3), 590–608.

Eck, T., B. Holben, J. Reid, O. Dubovik, A. Smirnov, N. O'Neill, I. Slutsker, and S. Kinne (1999), Wavelength dependence of the optical depth of biomass burning, urban, and desert dust aerosols, *J. Geophys. Res.*, *104*(D24), 31,333–31,349, doi:10.1029/1999JD900923.

Eck, T. F., B. Holben, A. Sinyuk, R. Pinker, P. Goloub, H. Chen, B. Chatenet, Z. Li, R. P. Singh, and S. N. Tripathi (2010), Climatological aspects of the optical properties of fine/coarse mode aerosol mixtures, *J. Geophys. Res.*, *115*, D19205, doi:10.1029/2010JD014002.

Elvidge, C. D., M. Zhizhin, K. Baugh, F.-C. Hsu, and T. Ghosh (2015), Methods for global survey of natural gas flaring from visible infrared imaging radiometer suite data, *Energies*, *9*(1), 14.

Ezeh, G. C., I. B. Obioh, O. I. Asubiojo, and O. E. Abiye (2012), PIXE characterization of PM_{10} and $PM_{2.5}$ particulates sizes collected in Ikoyi Lagos, Nigeria, *Toxicol. Environ. Chem.*, *94*(5), 884–894.

Fawole, O., X.-M. Cai, and A. MacKenzie (2016), Gas flaring and resultant air pollution: A review focusing on black carbon, *Environ. Pollut.*, *216*, 182–197, doi:10.1016/j.envpol.2016.05.075.

Giles, D. M., B. N. Holben, T. F. Eck, A. Sinyuk, A. Smirnov, I. Slutsker, R. Dickerson, A. Thompson, and J. Schafer (2012), An analysis of AERONET aerosol absorption properties and classifications representative of aerosol source regions, *J. Geophys. Res.*, *117*, D17203, doi:10.1029/2012JD018127.

Giwa, S. O., O. O. Adama, and O. O. Akinyemi (2014), Baseline black carbon emissions for gas flaring in the Niger Delta region of Nigeria, *J. Nat. Gas Sci. Eng.*, *20*, 373–379.

Holben, B., T. Eck, I. Slutsker, D. Tanre, J. Buis, A. Setzer, E. Vermote, J. Reagan, Y. Kaufman, and T. Nakajima (1998), AERONET—A federated instrument network and data archive for aerosol characterization, *Remote Sens. Environ.*, *66*(1), 1–16.

Holben, B., D. Tanre, A. Smirnov, T. Eck, I. Slutsker, N. Abuhassan, W. Newcomb, J. Schafer, B. Chatenet, and F. Lavenu (2001), An emerging ground-based aerosol climatology: Aerosol optical depth from AERONET, *J. Geophys. Res.*, *106*(D11), 12,067–12,097, doi:10.1029/2001JD900014.

Holben, B., T. Eck, I. Slutsker, A. Smirnov, A. Sinyuk, J. Schafer, D. Giles, and O. Dubovik (2006), AERONET's version 2.0 quality assurance criteria, Asia-Pacific remote sensing symposium. International Society for Optics and Photonics, pp. 64080Q-64080Q-14.

Huang, K., J. S. Fu, V. Y. Prikhodko, J. M. Storey, A. Romanov, E. L. Hodson, J. Cresko, I. Morozova, Y. Ignatieva, and J. Cabaniss (2015), Russian anthropogenic black carbon: Emission reconstruction and Arctic black carbon simulation, *J. Geophys. Res. Atmos.*, *120*, 11,306–11,333, doi:10.1002/2015JD023358.

Ite, A. E., and U. J. Ibok (2013), Gas flaring and venting associated with petroleum exploration and production in the Nigeria's Niger Delta, *Am. J. Environ. Protect.*, *1*(4), 70–77.

Kim, D., M. Chin, H. Yu, T. Eck, A. Sinyuk, A. Smirnov, and B. Holben (2011), Dust optical properties over North Africa and Arabian Peninsula derived from the AERONET dataset, *Atmos. Chem. Phys.*, *11*(20), 10,733–10,741.

Koch, D., M. Schulz, S. Kinne, C. McNaughton, J. Spackman, Y. Balkanski, S. Bauer, T. Berntsen, T. C. Bond, and O. Boucher (2009), Evaluation of black carbon estimations in global aerosol models, *Atmos. Chem. Phys.*, *9*(22), 9001–9026.

Lee, J., J. Kim, C. Song, S. Kim, Y. Chun, B. Sohn, and B. Holben (2010), Characteristics of aerosol types from AERONET Sunphotometer measurements, *Atmos. Environ.*, *44*(26), 3110–3117.

Lim, S., M. Lee, S.-W. Kim, S.-C. Yoon, G. Lee, and Y. Lee (2014), Absorption and scattering properties of organic carbon versus sulfate dominant aerosols at Gosan climate observatory in Northeast Asia, *Atmos. Chem. Phys.*, *14*(15), 7781–7793.

Methven, J. (1997), Offline trajectories: Calculation and accuracy UGAMP.
Methven, J., M. Evans, P. Simmonds, and G. Spain (2001), Estimating relationships between air mass origin and chemical composition, *J. Geophys. Res.*, *106*(D5), 5005–5019, doi:10.1029/2000JD900694.
Mielonen, T., A. Arola, M. Komppula, J. Kukkonen, J. Koskinen, G. de Leeuw, and K. Lehtinen (2009), Comparison of CALIOP level 2 aerosol subtypes to aerosol types derived from AERONET inversion data, *Geophys. Res. Lett.*, *36*, L18804, doi:10.1029/2009GL039609.
Milinevsky, G., V. Danylevsky, V. Bovchaliuk, A. Bovchaliuk, P. Goloub, O. Dubovik, V. Kabashnikov, A. Chaikovsky, N. Miatselskaya, and M. Mishchenko (2014), Aerosol seasonal variations over urban-industrial regions in Ukraine according to AERONET and POLDER measurements, *Atmos. Meas. Tech.*, *7*, 1459–1474.
Obioh, I., G. Ezeh, O. Abiye, A. Alpha, E. Ojo, and A. Ganiyu (2013), Atmospheric particulate matter in Nigerian megacities, *Toxicol. Environ. Chem.*, *95*(3), 379–385.
Olaniran, O. (1982), The physiological climate of Ilorin, Nigeria. Archives for meteorology, *Archives Meteorol. Geophys. Bioclimatol. Ser. B*, *31*(3), 287–299.
Omar, A. H., J. G. Won, D. M. Winker, S. C. Yoon, O. Dubovik, and M. P. McCormick (2005), Development of global aerosol models using cluster analysis of Aerosol Robotic Network (AERONET) measurements, *J. Geophys. Res.*, *110*, D10S14, doi:10.1029/2004JD004874.
O'Neill, N., Eck, T., Smirnov, A., Holben, B. and Thulasiraman, S. (2003), Spectral discrimination of coarse and fine mode optical depth, *J. Geophys. Res.*, *108*(D17), 4559, doi:10.1029/2002JD002975.
Onyeuwaoma, N. D., O. K. Nwofor, T. C. Chineke, E. O. Eguaroje, and V. N. Dike (2015), Implications of MODIS impression of aerosol loading over urban and rural settlements in Nigeria: Possible links to energy consumption patterns in the country, *Atmos. Pollut. Res.*, *6*(3), 484–494.
Owoade, O. K., O. G. Fawole, F. S. Olise, L. T. Ogundele, H. B. Olaniyi, M. S. Almeida, M.-D. Ho, and P. K. Hopke (2013), Characterization and source identification of airborne particulate loadings at receptor site-classes of Lagos Mega-City, Nigeria, *J. Air Waste Manage.*, *63*(9), 1026–1035.
Pandithurai, G., R. Pinker, O. Dubovik, B. Holben, and T. Aro (2001), Remote sensing of aerosol optical characteristics in sub-Sahel, West Africa, *J. Geophys. Res.*, *106*(D22), 28,347–28,356, doi:10.1029/2001JD900234.
Pinker, R., H. Liu, S. Osborne, and C. Akoshile (2010), Radiative effects of aerosols in sub-Sahel Africa: Dust and biomass burning, *J. Geophys. Res.*, *115*, D15205, doi:10.1029/2009JD013335.
Roberts, G., M. Wooster, and E. Lagoudakis (2009), Annual and diurnal African biomass burning temporal dynamics, *Biogeosciences*, *6*(5).
Rozwadowska, A., T. Zieliński, T. Petelski, and P. Sobolewski (2010), Cluster analysis of the impact of air back-trajectories on aerosol optical properties at Hornsund, Spitsbergen, *Atmos. Chem. Phys.*, *10*(3), 877–893.
Russell, P. B., M. Kacenelenbogen, J. M. Livingston, O. P. Hasekamp, S. P. Burton, G. L. Schuster, M. S. Johnson, K. D. Knobelspiesse, J. Redemann, and S. Ramachandran (2014), A multiparameter aerosol classification method and its application to retrievals from space-borne polarimetry, *J. Geophys. Res. Atmos.*, *119*, 9838–9863, doi:10.1002/2013JD021411.
Russell, P., R. Bergstrom, Y. Shinozuka, A. Clarke, P. DeCarlo, J. Jimenez, J. Livingston, J. Redemann, O. Dubovik, and A. Strawa (2010), Absorption Angström Exponent in AERONET and related data as an indicator of aerosol composition, *Atmos. Chem. Phys.*, *10*(3), 1155–1169.
Sato, M., J. Hansen, D. Koch, A. Lacis, R. Ruedy, O. Dubovik, B. Holben, M. Chin, and T. Novakov (2003), Global atmospheric black carbon inferred from AERONET, *Proc. Natl. Acad. Sci. U.S.A.*, *100*(11), 6319–6324.
Schuster, G. L., O. Dubovik, and B. N. Holben (2006), Angström Exponent and bimodal aerosol size distributions, *J. Geophys. Res.*, *111*, D07207, doi:10.1029/2005JD006328.
Shindell, D., M. Chin, F. Dentener, R. Doherty, G. Faluvegi, A. M. Fiore, P. Hess, D. Koch, I. MacKenzie, and M. Sanderson (2008), A multi-model assessment of pollution transport to the Arctic, *Atmos. Chem. Phys.*, *8*(17), 5353–5372.
Smirnov, A., Holben, B., Eck, T., Slutsker, I., Chatenet, B. and Pinker, R. (2002), Diurnal variability of aerosol optical depth observed at AERONET (Aerosol Robotic Network) sites, *Geophys. Res. Lett.*, *29*, (23), 2115, doi:10.1029/2002GL016305.
Stier, P., J. Feichter, E. Roeckner, S. Kloster, and M. Esch (2006), The evolution of the global aerosol system in a transient climate simulation from 1860 to 2100, *Atmos. Chem. Phys.*, *6*(10), 3059–3076.
Sultan, B., and S. Janicot (2000), Abrupt shift of the ITCZ over West Africa and intra-seasonal variability, *Geophys. Res. Lett.*, *27*(20), 3353–3356, doi:10.1029/1999GL011285.
Sultan, B., and S. Janicot (2003), The West African monsoon dynamics. Part II: The "preonset" and "onset" of the summer monsoon, *J. Clim.*, *16*(21), 3407–3427.
Toledano, C., V. Cachorro, A. Berjon, A. De Frutos, M. Sorribas, B. De la Morena, and P. Goloub (2007), Aerosol optical depth and Ångström exponent climatology at El Arenosillo AERONET site (Huelva, Spain), *Q. J. R. Meteorol. Soc.*, *133*(624), 795–807.
Tunde, A., E. Adeleke, and E. Adeniyi (2013), Impact of climate variability on human health in Ilorin, Nigeria, *Environ. Nat. Resour. Res.*, *3*(1), 127.
U.S. Environmental Protection Agency (2012), Report to congress on black carbon. EPA-450/R-12-001, United States Environmental Protection Agency.